Article ID: 1000-7032(2022)06-0911-11

A Stable UV Photodetector Based on n-ZnS/p-CuSCN Nanofilm with High On/Off Ratio

WEI Yao-qi, QUAN Jia-le, ZHAO Qing-qiang,
ZHOU Ming-chen, HAN San-can*

(*College of Materials and Chemistry*, *University of Shanghai for Science and Technology*, *Shanghai* 200093, *China*)

* *Corresponding Author*, *E-mail*: *mickey3can@163. com*

Abstract: Herein, We fabricated a CuSCN nanofilm ultraviolet(UV) photodetector(PD) using an *in situ* growth method. When the bias is −1 V and the incident light is 350 nm, the on/off ratio of the CuSCN PD is ~94, and the rise/decay time is ~ 1. 41 s/1. 44 s. However, such a device still cannot be called a high-performance photodetector. To improve the optoelectronic properties of CuSCN nanofilm further, we fabricated a UV photodetector based on n-ZnS/p-CuSCN composite nanofilm and analyzed its morphology, composition, and properties. The photocurrent and dark current of the ZnS/CuSCN UV photodetectors are 1.22×10^{-5} A and 4.8×10^{-9} A, respectively(at −1 V, 350 nm). The ZnS/CuSCN nanofilms' on/off ratio of ~2 542 and rise/decay time is 0. 47 s/0. 48 s. Besides, the n-ZnS/p-CuSCN nanofilm UV PDs have the best responsivity and detectivity at 350 nm with 5. 17 mA/W and 1.32×10^{11} Jones, respectively. In addition, the n-ZnS/p-CuSCN composite film is stable at room temperature, which indicates its great potential as a high-performance UV photodetector.

Key words: photodetector; p-n junction; ZnS/CuSCN; on/off ratio

CLC number: TN23　　**Document code**: A　　**DOI**: 10. 37188/CJL. 20220069

一种基于 n-ZnS/p-CuSCN 纳米薄膜的高开关比和稳定性紫外光电探测器

魏瑶琪，全家乐，赵庆强，邹明琛，韩三灿*

（上海理工大学 材料与化学学院，上海　200093）

摘要：通过原位生长法制备了一种 CuSCN 纳米薄膜紫外光电探测器，在−1 V 偏压下，入射光为 350 nm 时，CuSCN 紫外光电探测器的开关比 ~ 94，响应/恢复时间~1.41 s/1.44 s。但这种器件仍不能称之为一种高性能的光电探测器。为进一步提高 CuSCN 纳米薄膜的光电性能，我们制备了一种基于 n-ZnS/p-CuSCN 复合薄膜的紫外光电探测器，并对制备的样品进行了形貌、成分和性能分析。结果显示，在−1 V 偏压下，入射波长为 350 nm 时，ZnS/CuSCN 紫外光电探测器表现出比 CuSCN 紫外光电探测器更高的光电流和更低的暗电流，分别为 1.22×10^{-5} A 和 4.8×10^{-9} A。基于 ZnS/CuSCN 纳米薄膜的紫外光电探测器开关比−2 542，响应/恢复时间为 0.47 s/0.48 s，在 350 nm 波长下具备最佳的响应度和探测率，分别为 5.17 mA/W 和 1.32×10^{11} Jones。此外，n-ZnS/p-CuSCN 复合薄膜在室温下性能稳定，具有作为高性能紫外探测器的潜力。

关　键　词：光电探测器；p-n 结；ZnS/CuSCN；开关比

收稿日期：2022-03-01；**修订日期**：2022-03-14

基金项目：国家自然科学基金(51802195)；上海市教委晨光学者项目(19CG53)资助

Supported by National Natural Science Foundation of China(51802195); Chenguang Scholar Project of Shanghai Education Commission(19CG53)

1 Introduction

Photodetectors are electronic devices that convert light signals into electrical signals and play an essential role in human life[1-2]. In particular, ultraviolet (UV) photodetectors (PDs) are widely used in optical communication, biosensing, photoelectric detection, and environmental monitoring[3-5]. It is commonly accepted that an excellent photodetector should have high sensitivity, high signal-to-noise ratio, high spectral selectivity, high speed, and high stability[6].

Several general wide bandgap semiconductors have been used for UV PDs in the past decade[7-8], such as GaN[9], ZnO[10], In_2O_3[11], CuSCN[12], *etc*. Especially, CuSCN is a broadband transparent p-type semiconductor with a bandgap of about 3.7 eV with excellent UV selectivity[13]. Many CuSCN nanofilm photodetectors have been reported to have high UV sensitivity and stability. Yang *et al*. [14] and Ka *et al*. [15] assembled a CuSCN-based UV PD with response/recovery time of 150 μs/30 μs and 6.7 μs/0.95 ms, respectively. However, the on/off ratio is not as good as expected, at 200 and 512. In recent years, Yan *et al*. [16] constructed a $Cs_2AgBiBr_6$/CuSCN photodetector with a high detectivity (1.03×10^{13} Jones) and high photocurrent (7×10^{-7} A), but the on/off ratio is still not ideal.

This paper has obtained CuSCN nanofilm by an *in situ* growth method. However, the rise/decay time (1.41 s/1.44 s) and the on/off ratio (~94) of the PD based on CuSCN are not ideal due to surface defects and crystallinity. Researchers have proposed several approaches to solve the above problems, including the introduction of Scotty junctions, heterojunctions[17-18], surface modifications[19], and size optimization[20]. Composites often exhibit superior performance over single materials due to heterojunctions and synergistic effects between materials[21-23]. Therefore, to obtain a high-performance CuSCN-based UV PD, we prefer an n-type semiconductor with the highest absorbance in the UV region as the composite.

Zinc sulfide (ZnS), a highly crystalline n-type semiconductor material, has good electrical and optical properties and is widely used in optoelectronic devices[24-27]. The bandgap of ZnS is about 3.6 eV[28], indicating its excellent UV selectivity and potential material for improving CuSCN UV PD's performance. Many ZnS PDs with different nanostructures have been demonstrated to exhibit excellent properties, such as thin films[29], nanowires[30], nanoarrays[31], quantum dots[32], *etc*. Reports on ZnS photodetectors show that responsibility of 0.1 mA/W and a rise/decay time of 0.35 s/0.07 s under UV irradiation[33]. Therefore, ZnS is a promising n-type material to build p-n junctions with CuSCN. In particular, the built-in electric field in the vicinity of the PN junction effectively promotes the separation of the current carrier[34-35]. The composites are expected to have faster responses and higher photocurrents, enabling high-performance photodetectors.

This work obtained *in situ* growth CuSCN nanofilm PDs (on/off ratio ~94, rise/decay time ~1.41 s/1.44 s). Subsequently, we fabricated a ZnS/CuSCN nanofilm photodetector with a high on/off ratio and stability based on the CuSCN nanofilm. Ultraviolet optoelectronic properties of PDs based on composite films have been improved. The on/off ratio of the ZnS/CuSCN PD is ~2 542, while the rise/decay time is 0.47 s/0.48 s (at −1 V, 350 nm). In addition, the responsivity and detection of the device are 5.17 mA/cm^2 and 1.32×10^{11} Jones, respectively. Therefore, ZnS/CuSCN device is expected to be a candidate for high-performance UV photodetectors.

2 Experiment

2.1 Synthesis of CuSCN Films

A copper foil (99.99% purity, 1 cm×1 cm) was cleaned in 0.1 mol/L HCl and then rinsed by ethanol and DIW, followed by air blow-drying. Then it was immersed in an alkaline solution for a while. Next, the sample was annealed at 500 ℃ for 1 h and kept for 1 h to obtain Cu_2O nanofilm. Used a constant flow of N_2 (99.99%) with 80 mL/min as protecting and carrier gas through the entire process. Finally, the Cu_2O was added to the KSCN solution (5 mmol/L) for 72 h at room temperature.

2.2 Synthesis of ZnS

$(NH_4)_2S$ aqueous solution (3.5 mL, 8%) was stirred at 60 ℃. Then 5 mmol $Zn(NO_3)_2 \cdot 6H_2O$ was dissolved in $(NH_4)_2S$ for 2 h, excess ethanol was added to the obtained solution, the product was collected by centrifugation at 10 000 r/min for 20 min, dried the ZnS powder in a high temperature drying oven for 2 h.

2.3 Fabrication of ZnS/CuSCN Films

The ZnS powder was dissolved in N, N-dimethylformamide (0.01 mol/L) and applied drops onto the surface of CuSCN film.

2.4 Characterization

Morphological electron microscopy (SEM, FEI Quanta 450FEG) of the samples was analyzed by scanning method. Transmission electron microscopy (TEM), high-resolution transmission electron microscopy (HRTEM), and high angle annular dark-field (HAADF) were also performed for transmission electron microscopy (Tecnai G2 F30). The phase structures were investigated by using X-ray diffraction (XRD, D8-Advance/Germany). In addition, EDS spectra of scanning transmission electron microscopy (STEM) mode were also used to study the distribution of elements. XPS was performed by a spectrometer (Thermo Scientific K-Alpha). Raman spectroscopy was tested on a LabRAM HR Evolution spectrometer with a 532 nm laser. UV-Vis was characterized by a UV-Vis diffuse reflectance spectrometer (UV-3600). The optoelectronic properties of the devices are described by a semiconductor characterization system (Keithley 4200-SCS).

3 Results and Discussion

The XRD patterns of ZnS and ZnS/CuSCN composites are shown in Fig. 1(a). Diffraction peaks appearing at 16°, 27.1°, 32.5°, 34.4°, 50.1°, 58.5° are caused by (006), (012), (0012), (018), (116), (027), match the standard peak of hexagonal CuSCN (JCPDS 73-1855). The diffraction peaks with 2θ values of 28.6°, 33.1°, 47.5°, 56.4° and 78.8° belong to the (002), (100), (112) and (210) crystal orientations of the ZnS cubic crystal structure, respectively. All peaks are perfectly matched, confirming the successful preparation of the uniform crystal structure. The ZnS was analyzed according to the reference card (JCPDS # 99-0097), as seen in Fig. S1. The XRD pattern of the ZnS/CuSCN nanofilm possesses peaks of both ZnS and CuSCN, which confirms the successful preparation of the ZnS/CuSCN nanofilm. Fig. 1(b) shows Raman spectra of ZnS/CuSCN film, which shows three different Raman peaks. The ZnS/CuSCN nanofilm offers three Raman peaks at 260, 350, 2 175 cm^{-1}. The peak of 2 175 cm^{-1} is attributed to CuSCN. Fig. S2 is the Raman spectrum of a single CuSCN, showing that there is only one Raman peak of CuSCN located at 2 174 cm^{-1}, which is almost consistent with the Raman peak of CuSCN in ZnS/CuSCN composites. Fig. S3 shows the Raman spectra of ZnS, further conducted to confirm ZnS formation in the ZnS/CuSCN nanocomposite. There are two apparent peaks at 260 cm^{-1} and 350 cm^{-1}, ascribed to the E1/A1(TO) and E1/A1 (LO) vibrational modes of the single ZnS phase[36-37]. The absence of the A1 (TO) phonon peak in the

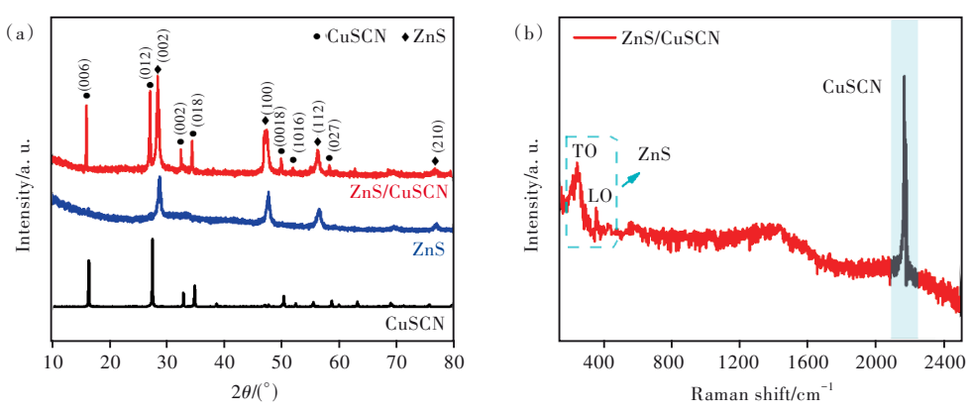

Fig. 1　(a) The XRD patterns of ZnS/CuSCN sample. (b) Raman spectra of ZnS/CuSCN.

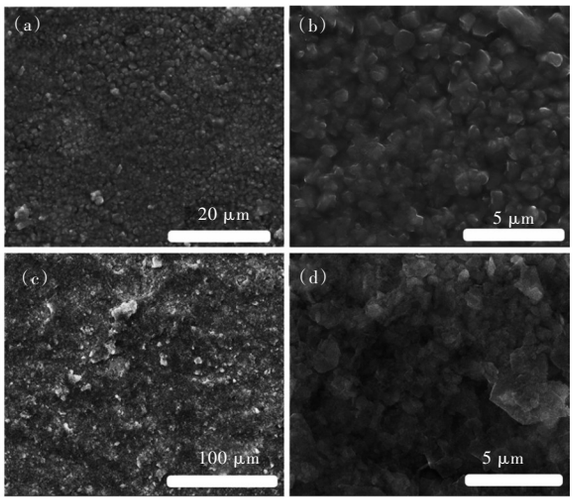

Fig. 2 (a)-(b) SEM images of CuSCN nanofilm. (c)-(d) SEM images of ZnS/CuSCN composite.

Raman spectrum proves that the synthesized ZnS is a pure ZB (zinc-blende structure) phase. The broad features at 350–450 cm^{-1} are related to the second-order Raman scattering, including the combination and overtone of several ZnS phonon modes. The peak position of the ZnS bulk phonon modes is close to the reported bulk values, indicating the excellent crystal quality with strain-free growth of ZnS[38].

Fig. 2(a)-(d) show the SEM images of CuSCN and ZnS/CuSCN. The surface of pure CuSCN exhibits large-area bulk stacks, a high-density structure, and is very uniform. In addition, Fig. 2(c)-(d) indicate that the ZnS film is deposited on the surface of the CuSCN, which is more dense and uniform than pure CuSCN. This structure is beneficial to electron transfer and has certain structural advantages compared with CuSCN.

The HRTEM images in Fig. 3(a) show different lattice spacing of 0.33 nm and 0.295 nm on the CuSCN surface, corresponding to the (012) and (018) planes of CuSCN, respectively, which are consistent with the XRD results. The EDX analysis in Fig. 3(b) shows almost the same elemental distribution of Cu, S, N, and C in CuSCN, which further confirms the presence of CuSCN substrates.

The UV-Vis diffuse reflectance spectra (DRS) of CuSCN film, ZnS, and ZnS/CuSCN film are shown in Fig. 4(a)-(c). They showed strong absorption in the ultraviolet region. Fig. 4(a)-(c) inset images show $(\alpha h\nu)^2$ *versus* photon energy $h\nu$ plots of CuSCN, ZnS, and ZnS/CuSCN, respectively. According to the UV-Vis absorption spectrum analysis and the formula calculation, the E_g of CuSCN, ZnS, and ZnS/CuSCN is 3.61, 3.62, 3.71 eV, respectively. The calculated E_g of ZnS/CuSCN is more significant than ZnS. The above analysis proves that ZnS/CuSCN

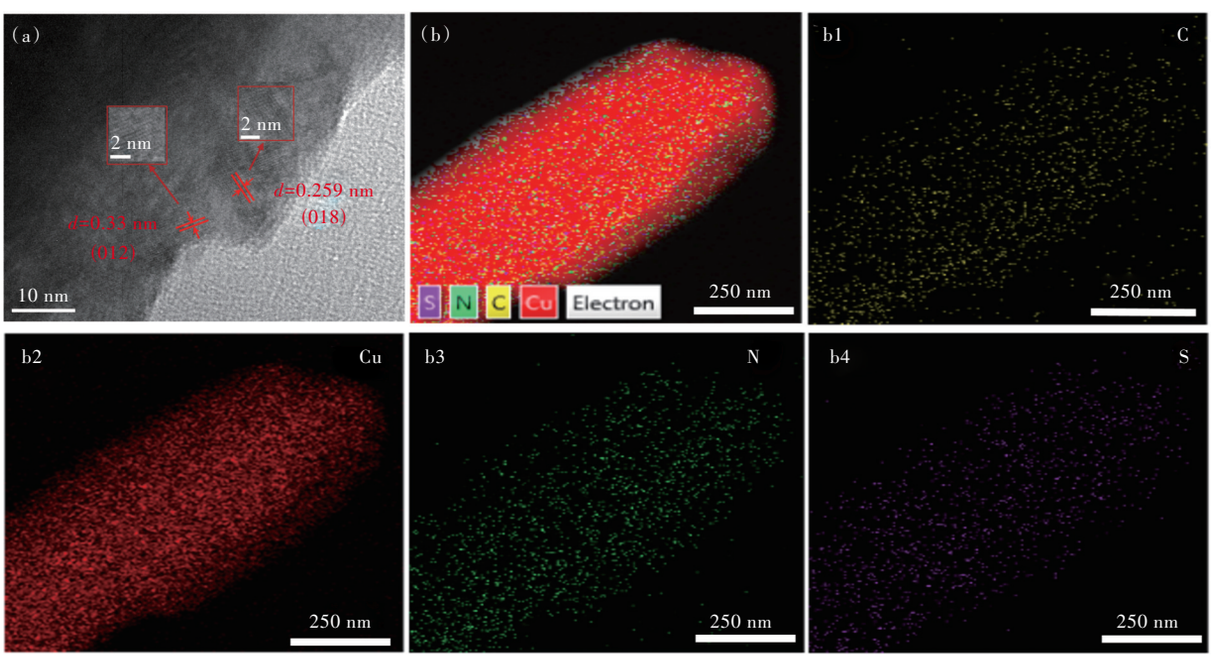

Fig. 3 (a) HRTEM images of CuSCN. (b) HAADF-STEM images of CuSCN, and the corresponding EDX mapping of C, Cu, N, and S elements.

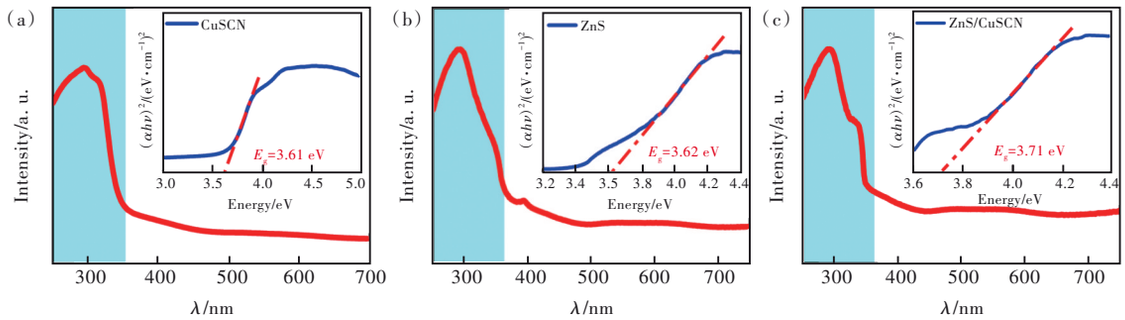

Fig. 4　(a)-(c) The UV-Vis DRS and the corresponding $(\alpha h\nu)^2$ *versus* photon energy plots of the activated CuSCN, ZnS and ZnS/CuSCN.

has excellent application potential for UV detection. XPS measurement was employed to analyze the elementary composition of ZnS/CuSCN. Fig. 5(a) confirmed the existence of Cu, S, C, N, and Zn. The binding energies of the C1s spectrum of ZnS/CuSCN are appeared at 285.2 eV and 285.8 eV, respectively, in Fig. 5(b), which were ascribed to the presence of C in CuSCN. Besides, the peak at 284.6 eV is attributed to extraneous carbon-based pollutants. Fig. 5(c) showed the N 1s spectrum of ZnS/CuSCN. There are two peaks distributed at 398.2 eV and 399.8 eV, respectively. Fig. 5(d) showed the S 2p XPS spectra for ZnS/CuSCN, the S $2p_{1/2}$ and S $2P_{3/2}$ occurred at 164.5 eV and 163.2 eV[39]. And the error is within ± 0.2 eV between them, attributed to the S in CuSCN. Fig. 5(c) shows the core energy levels in the N 1s spectra of ZnS/CuSCN are located at 398.2 eV and 399.8 eV, respectively, and Fig. 5(e) depicts the high-resolution spectrum of Cu 2p. The fitted peaks at 952.45 eV (Cu $2p_{1/2}$) and at 932.6 eV (Cu $2p_{3/2}$) match well with that of Cu^{+} [40-42]. Fig. 5(f) shows Zn 2p XPS spectrum of ZnS/CuSCN, splits into Zn $2p_{3/2}$(1 022.1 eV) and Zn $2p_{1/2}$(1 044.9 eV)[42-43], which is consistent with that of Zn^{2+}. In summary, XPS analysis confirms the successful recombination of ZnS/CuSCN, providing a basis for the possibility of forming high-quality p-n junctions of ZnS/CuSCN.

The photoelectric properties were investigated using a two-probe method at room temperature regarding ZnS/CuSCN composite PDs by constructing silver paste with a small area as the electrodes

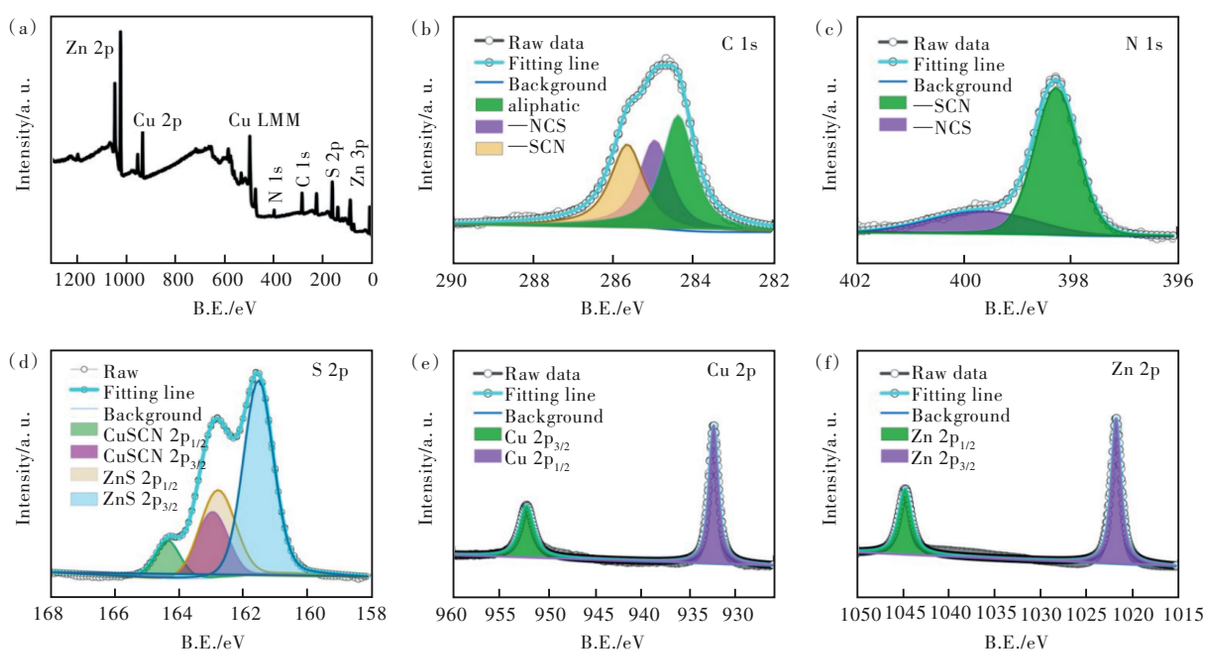

Fig. 5　XPS spectra. (a) Survey spectrum of ZnS/CuSCN. (b) ZnS/CuSCN C1 spectra. (c) ZnS/CuSCN N 1s spectra. (d) ZnS/CuSCN S 2p spectra. (e) ZnS/CuSCN Cu 2p spectra. (f) ZnS /CuSCN Zn 2p spectra.

(~ 1 cm^2). Fig. 6(a) shows typical current-voltage (*I-V*) curves of ZnS/CuSCN and CuSCN devices under −1−1 V bias, irradiated with 350 nm UV light (~2.36 mW/cm^2). The *I-V* curves indicate that CuSCN composite with ZnS improves the optoelectronic performance compared with CuSCN. Notably, the *I-V* curve of the ZnS/CuSCN device exhibits asymmetry under forwarding bias, which confirms that the ZnS/CuSCN devices form a high-quality p-n junction[44]. The photocurrent of ZnS/CuSCN is 1.22×10^{-5} A, and the dark current is 4.8×10^{-9} A. The dark current of CuSCN is 3.01×10^{-8} A. Compared with CuSCN PDs, the decrease in the dark current of ZnS/CuSCN PDs due to the formation of a denser film on the surface after adding ZnS, which reduces the surface defects. Thus, it reduces the ZnS/CuSCN device's surface recombination current and surface leakage current[45], confirms that the ZnS/CuSCN nanofilm UV photodetector is excellent. Fig. 6(c) shows the on/off ratio (I_{light}/I_{dark}) of the ZnS/CuSCN composite films is 2 542, which is greatly improved compared with the CuSCN nanofilm (~94), is due to the decrease of dark current and the increase of photocurrent after CuSCN composite ZnS. The ZnS/CuSCN PDs show an excellent on/off ratio, about one order of magnitude higher than CuSCN PDs. The ZnS/CuSCN PDs offer an excellent on/off ratio, approximately one order of magnitude higher than that of CuSCN PDs. The responsivity is defined as $R = I_{ph}/P_{in}$, where I_{ph} is $I_{light}-I_{light}$, and P_{in} is the average optical power irradiating to the sample, which indicates how much photocurrent can be produced by unit incident power on the photodetector. The ZnS/CuSCN responds well to UV light in the UVA band, demonstrating the best responsivity of 5.17 mA/W upon 350 nm UV irradiation. The detectivity is one of the most critical parameters for photodetectors, defined by the equation, $D^*=RA^{1/2}/(2eI_{dark})^{1/2}$, where A is the effective photosensitive area of the device. The ZnS/CuSCN shows a high detectivity of $D^*=1.32\times10^{11}$

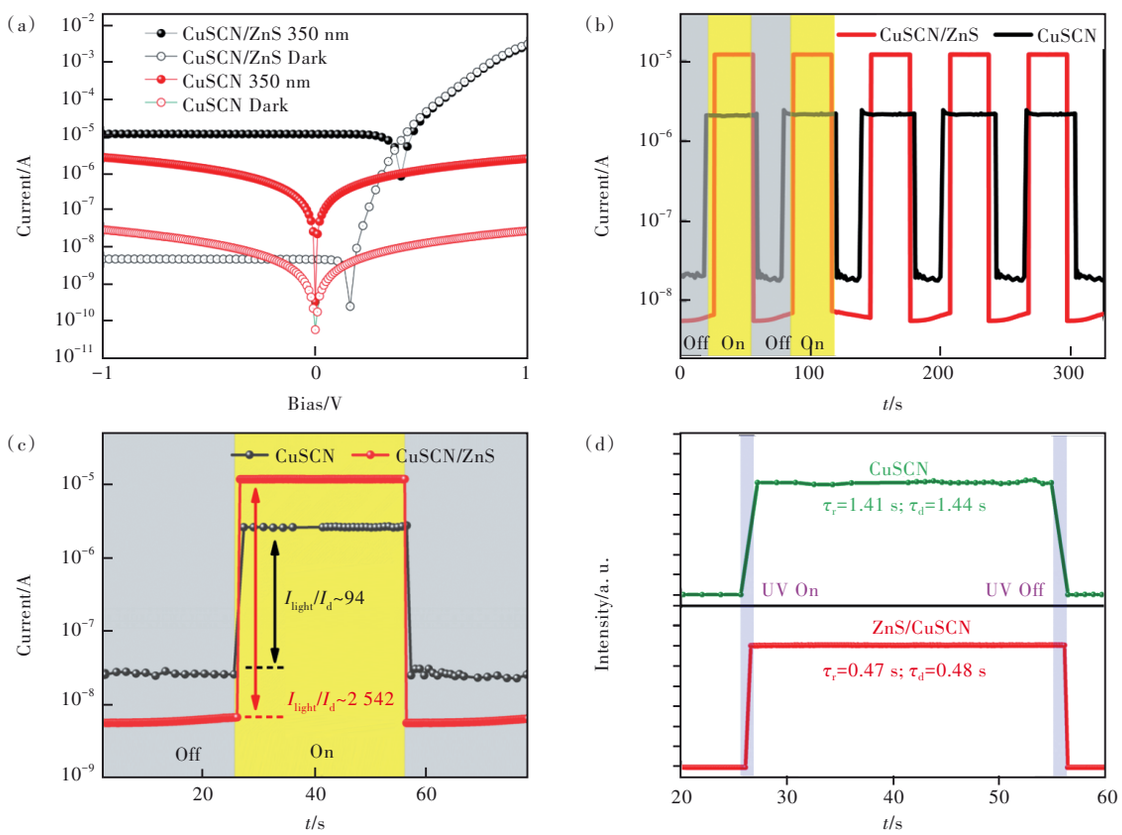

Fig. 6 (a) The *I-V* curves of ZnS/CuSCN PD and pure CuSCN PD under dark and light illumination of 350 nm. (b) *I-t* curves of ZnS/CuSCN PD and CuSCN PD with periodical on/off switching upon 350 nm UV light illumination under −1 V bias. (c) A single period of the *I-t* curve on a semilogarithmic plot of ZnS/CuSCN PD and CuSCN PD. (d) Response speed curves of CuSCN/ZnS PD and CuSCN PD.

Jones towards 350 nm. Moreover, these ZnS/CuSCN composite films maintain excellent stability at room temperature and last for more than 30 d without significant decay, as shown in Fig. S4. Five response recovery cycles of the ZnS/CuSCN PD are shown in Fig. 6(b), which also confirms the stability and repeatability of the device. But it is shown in Fig. 6(b) that the dark current of ZnS/CuSCN PDs does not offer a horizontal straight line. Possible reasons for this problem might be the instability of the contact junction region between the ZnS and CuSCN. Fig. 6(d) shows that the rise time and decay time of the ZnS/CuSCN PDs are 0.47 s and 0.48 s, respectively. However, the rise time and decay time of CuSCN PDs are 1.41 s and 1.44 s, respectively, which suggests that ZnS/CuSCN nanofilm respond faster.

The responsivity is an essential parameter to the sensitivity of the photodetector. According to Fig. 7(a), the ZnS/CuSCN PD exhibits outstanding UV photodetector performance. The results in Fig. 7(b) indicate that the responsivity and detectivity of the ZnS/CuSCN device increased gradually from 300 nm to 350 nm. The ZnS/CuSCN device has the best responsivity of 5.17 mA/W and D^* of 1.32×10^{11} Jones when using 350 nm light illumination. Fig. 7(c)

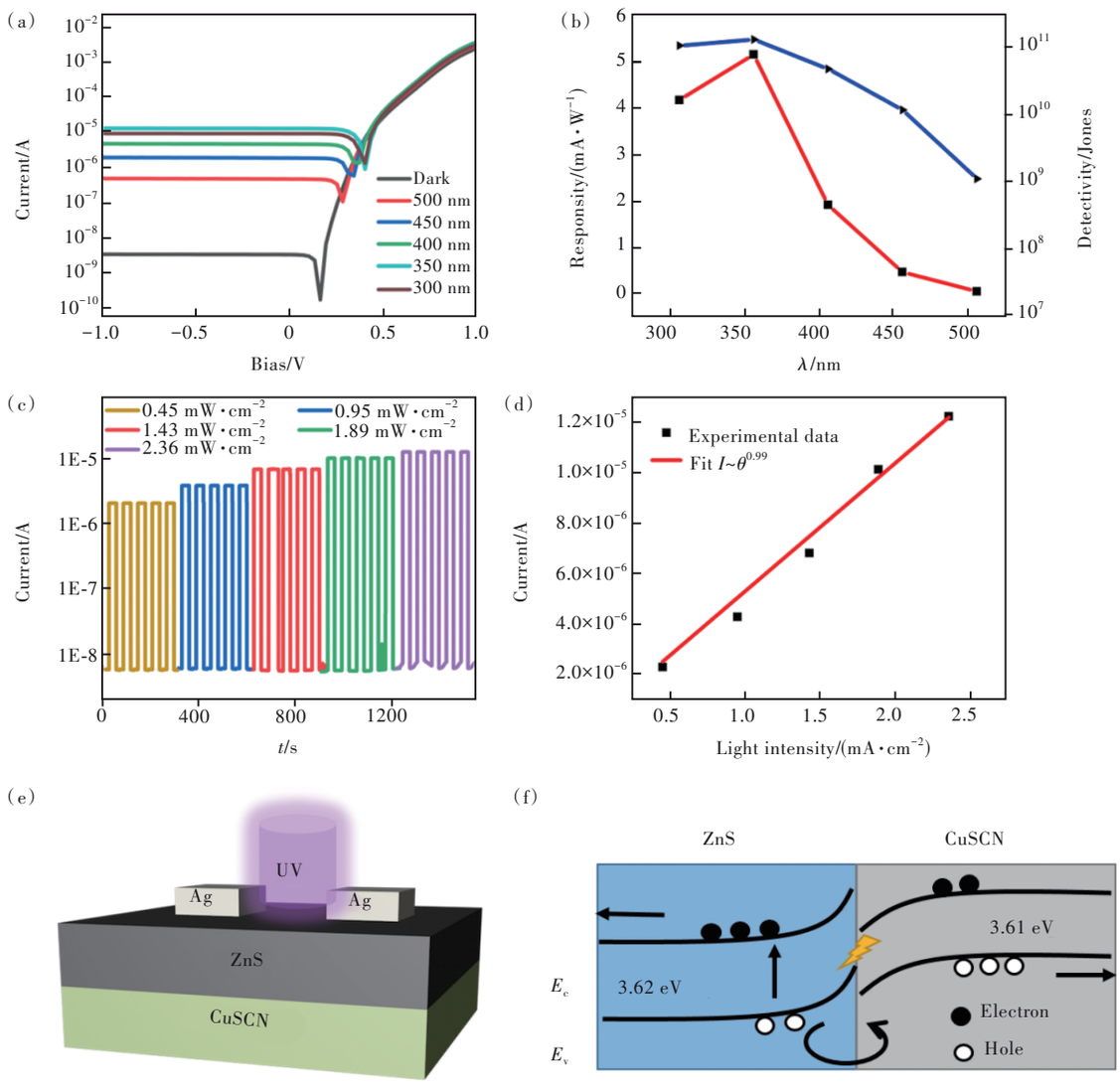

Fig.7　Photoelectric properties of ZnS/CuSCN. (a) *I-V* curves under dark and light illumination of 300, 350, 400, 450, 500 nm. (b) Spectral responsivity and D^* of ZnS/CuSCN. (c) *I-t* curves at −1 V bias upon 350 nm light illumination at different light intensities. (d) Corresponding fitting curves for the relationship between the photocurrent and the light intensity. (e) Schematic representations of the device. (f) The energy band alignment of the various layers in the ZnS/CuSCN.

shows the (current-time) I-t curve of the ZnS/CuSCN photodetectors at −1 V, the incident wavelength is 350 nm, under different optical densities (0.45, 0.95 , 1.43, 1.89, 2.36 mW/cm^2), the corresponding photocurrent values are 2.26×10^{-6}, 4.25×10^{-6}, 6.79×10^{-6}, 1.01×10^{-5}, 1.22×10^{-5} A, respectively, indicating that the photocurrent is proportional to the light intensity density. The above results show that the ZnS/CuSCN UV PDs are still highly stable even when operated at different powers. Fig. 7(d) shows that the responsivity of the ZnS/CuSCN PD is proportional to the optical power, calculated by exponential fitting. The value of θ is 0.99. Compared with recent reports on p-type PDs, ZnS/CuSCN device's on/off ratio is outstanding (Tab. 1), and the all-around performance is better than other devices. Fig. 7(e)-(f) shows schematic diagrams and corresponding theoretical band alignments of the ZnS/CuSCN devices. In the UV light test, UV light was first irradiated on the ZnS layer on the ZnS/CuSCN nanofilm and then reached the underlying CuSCN. ZnS has efficient electron mobility and can serve as an outer layer to provide an efficient transport path for photogenerated electrons. Meanwhile, the ZnS/CuSCN nanofilm belongs to the polycrystalline structure with more defects and interface states. Carriers are easily recombined through defects in transport and interfacial states. More importantly, the gradient energy level formed between ZnS and CuSCN facilitates an effective charge separation process and suppresses carrier recombination, desirable for a high-performance UV PD.

Tab. 1 The characteristic parameters of p-type PDs in the literature

Photodetector	Wavelength/nm	Bias/V	On/Off ratio	Responsivity/ (mA·W^{-1})	Detectivity (D^*)/Jones	τ_r/τ_d/s	Ref.
Pbs-QDs/CuSCN	532	1	200	79	7×10^{10}	150/30 μs	[15]
SnO_2/CuZnS	300	3	1 300	27.6	5.41×10^{11}	0.045/1.17 ms	[46]
ZnO-CuI/CuSCN	365	0	512	8.7 μA·cm^{-2}	—	0.5/0.1	[14]
FTO/perovskite/CuSCN/Ag	750	10	333.3	1.6	1.03×10^{13}	—	[16]
NiO/Ga_2O_3	254	0	122	57 μA·W^{-1}	5.45×10^{9}	0.34/3.56	[47]
ZnO:Cu	365	5	2 080	—	—	9.2/5.0	[48]
$CuGaS_2$	254	10	1.35	5.1×10^{3}	1.67×10^{11}	1.8/10.1	[49]
GaN/Si	325	0	325	132	2.4×10^{10}	67/24 ms	[50]
CuSCN	350	−1	~94	—	—	1.41/1.44	This work
ZnS/CuSCN	350	−1	~2 542	5.17	1.32×10^{11}	0.47/0.48	This work

4 Conclusion

In conclusion, we have developed a high-performance UV photodetector based on a ZnS/CuSCN p-n heterojunction. The on/off ratio of ZnS/CuSCN UV PD compared to CuSCN UV PD has been dramatically increased from the previous 94 times on/off ratio to 2 542 times. The ZnS/CuSCN UV PD decreases the dark current to 4.8×10^{-9} A and improves its photocurrent to 1.22×10^{-5} A. Moreover, the ZnS/CuSCN PD has the best responsivity and detectivity of 5.17 mA/W and 1.32×10^{11} Jones (at −1 V, 350 nm). In addition, the rise/decay time of ZnS/CuSCN PD is 0.47 s/0.48 s. ZnS/CuSCN PD also shows good cycling stability at different power levels. The results reported here provide a facile route to fabricate CuSCN-based UV photodetectors with high sensitivity, speed, and stability and lay a solid foundation for subsequent applications.

Supplementary Information and Response Letter are available for this paper at: http://cjl.lightpublishing.cn/thesisDetails#10.37188/CJL.20220069.

References:

[1] 韩悦,李国辉,梁强兵,等. 全无机钙钛矿 CsPbX_3纳米晶的研究进展[J]. 发光学报, 2020,41(5):542-556.

HAN Y, LI G H, LIANG Q B, *et al.* Advances of all-inorganic perovskite $CsPbX_3$ nanocrystals [J]. *Chin. J. Lumin.*, 2020, 41(5): 542-556. (in Chinese)

[2] 张翼鹏, 王雪, 纪佩璇, 等. 不同响应机制下的石墨烯基光电探测器研究进展 [J]. 发光学报, 2022, 43(4): 552-575.
ZHANG Y P, WANG X, JI P X, *et al.* Research progress of graphene based photodetectors under different response mechanisms [J]. *Chin. J. Lumin.*, 2022, 43(4): 552-575. (in Chinese)

[3] CHEN J X, OUYANG W X, YANG W, *et al.* Recent progress of heterojunction ultraviolet photodetectors: materials, integrations, and applications [J]. *Adv. Funct. Mater.*, 2020, 30(16): 1909909.

[4] SHAO D L, QIN L Q, SAWYER S. Near ultraviolet photodetector fabricated from polyvinyl-alcohol coated In_2O_3 nanoparticles [J]. *Appl. Surf. Sci.*, 2012, 261: 123-127.

[5] CAI S, XU X J, YANG W, *et al.* Materials and designs for wearable photodetectors [J]. *Adv. Mater.*, 2019, 31(18): 1808138-1-15.

[6] SANG L W, LIAO M Y, SUMIYA M. A comprehensive review of semiconductor ultraviolet photodetectors: from thin film to one-dimensional nanostructures [J]. *Sensors(Basel)*, 2013, 13(8): 482-518.

[7] CHEN H Y, LIU H, ZHANG Z M, *et al.* Nanostructured photodetectors: from ultraviolet to terahertz [J]. *Adv. Mater.*, 2016, 28(3): 403-433.

[8] XIA F N, MUELLER T, LIN Y M, *et al.* Ultrafast graphene photodetector [J]. *Nat. Nanotechnol.*, 2009, 4(12): 839-843.

[9] LIU L, YANG C, PATANÈ A, *et al.* High-detectivity ultraviolet photodetectors based on laterally mesoporous GaN [J]. *Nanoscale*, 2017, 9(24): 8142-8148.

[10] 李超群, 陈洪宇, 张振中, 等. 电极间距对ZnO基MSM紫外光电探测器性能的影响 [J]. 发光学报, 2014, 35(10): 1172-1175.
LI C Q, CHEN H Y, ZHANG Z Z, *et al.* Effect of electrode spacing on the properties of ZnO based MSM ultraviolet photodetector [J]. *Chin. J. Lumin.*, 2014, 35(10): 1172-1175. (in Chinese)

[11] 陈雪, 魏志鹏. 具有高光开关比和高响应度的单根In_2O_3纳米线紫外光电晶体管 [J]. 发光学报, 2021, 42(2): 208-214.
CHEN X, WEI Z P. Single In_2O_3 nanowire ultraviolet phototransistor with high optical on-off ratio and high responsivity [J]. *Chin. J. Lumin.*, 2021, 42(2): 208-214. (in Chinese)

[12] HATCH S M, BRISCOE J, DUNN S. A self-powered ZnO-nanorod/CuSCN UV photodetector exhibiting rapid response [J]. *Adv. Mater.*, 2013, 25(6): 867-871.

[13] WYATT-MOON G, GEORGIADOU D G, SEMPLE J, *et al.* Deep ultraviolet Copper(Ⅰ) thiocyanate (CuSCN) photodetectors based on coplanar nanogap electrodes fabricated *via* adhesion lithography [J]. *ACS Appl. Mater. Interfaces*, 2017, 9(48): 41965-41972.

[14] YANG Z, WANG M Q, DING J J, *et al.* Semi-transparent ZnO-CuI/CuSCN photodiode detector with narrow-band UV photoresponse [J]. *ACS Appl. Mater. Interfaces*, 2015, 7(38): 21235-21244.

[15] KA I, GERLEIN L F, ASUO I M, *et al.* Solution-processed p-type copper thiocyanate (CuSCN) enhanced sensitivity of PbS-quantum-dots-based photodiode [J]. *ACS Photonics*, 2020, 7(7): 1628-1635.

[16] YAN G H, JI Z, LI Z W, *et al.* All-inorganic $Cs_2AgBiBr_6$/CuSCN-based photodetectors for weak light imaging [J]. *Sci. China. Mater.*, 2020, 64(1): 198-208.

[17] HU K, TENG F, ZHENG L X, *et al.* Binary response Se/ZnO p-n heterojunction UV photodetector with high on/off ratio and fast speed [J]. *Laser Photonics Rev.*, 2017, 11(1): 1600257-1-7.

[18] YAN F G, WEI Z M, WEI X, *et al.* Toward high-performance photodetectors based on 2D materials: strategy on methods [J]. *Small Methods*, 2018, 2(5): 1700349-1-14.

[19] YANG W, HU K, TENG F, *et al.* High-performance silicon-compatible large-area UV-to-visible broadband photodetector based on integrated lattice-matched type Ⅱ Se/n-Si heterojunctions [J]. *Nano Lett.*, 2018, 18(8): 4697-4703.

[20] HU K, CHEN H Y, JIANG M M, *et al.* Broadband photoresponse enhancement of a high-performance *t*-se microtube photodetector by plasmonic metallic nanoparticles [J]. *Adv. Funct. Mater.*, 2016, 26(36): 6641-6648.

[21] CHEN C, XIE X Q, ANASORI B, *et al.* MoS_2-on-MXene heterostructures as highly reversible anode materials for lithium-ion

batteries [J]. *Angew. Chem.*, 2018,57(7):1846-1850.

[22] KWAK J Y, HWANG J, CALDERON B, *et al*. Electrical characteristics of multilayer MoS_2 FET's with MoS_2/graphene heterojunction contacts [J]. *Nano Lett.*, 2014,14(8):4511-4516.

[23] TIAN W, SUN H X, CHEN L, *et al*. Low-dimensional nanomaterial/Si heterostructure-based photodetectors [J]. *InfoMat.*, 2019,1(2):140-163.

[24] LI X, GAO S Y, WANG G N, *et al*. A self-powered ultraviolet photodetector based on TiO_2/Ag/ZnS nanotubes with high stability and fast response [J]. *J. Mater. Chem.* C, 2020,8(4):1353-1358.

[25] LI F, XIA Z G, LIU Q L. Controllable synthesis and optical properties of ZnS: Mn^{2+}/ZnS/ZnS: Cu^{2+}/ZnS core/multi-shell quantum dots towards efficient white light emission [J]. *ACS Appl. Mater. Interfaces*, 2017,9(11):9833-9839.

[26] ARJUNAN S, KAVITHA H P, PONNUSAMY S, *et al*. ZnS/CuS nanocomposites: an effective strategy to transform UV active ZnS to UV and Vis light active ZnS [J]. *J. Mater. Sci: Mater Electoron.*, 2016,27(9):9022-9033.

[27] SEPALAGE G A, MEYER S, PASCOE A R, *et al*. A facile deposition method for CuSCN: exploring the influence of CuSCN on *J-V* hysteresis in planar perovskite solar cells [J]. *Nano Energy*, 2017,32:310-319.

[28] ALTIN İ, POLAT İ, BACAKSIZ E, *et al*. ZnO and ZnS microrods coated on glass and photocatalytic activity [J]. *Appl. Surf. Sci.*, 2012,258(11): 4861-4865.

[29] ZHU Y, ZHANG Y F, YAN L M, *et al*. Novel ultraviolet photodetector with ultrahigh photosensitivity employing SILAR-deposited ZnS film on MgZnO [J]. *J. Alloys Compd.*, 2020,832: 155022-1-7.

[30] ZHANG K, DING J, LOU Z, *et al*. Heterostructured ZnS/InP nanowires for rigid/flexible ultraviolet photodetectors with enhanced performance [J]. *Nanoscale*, 2017,9(40): 15416-15422.

[31] LIN H L, WEI L, WU C C, *et al*. High-performance self-powered photodetectors based on ZnO/ZnS core-shell nanorod arrays [J]. *Nanoscale Res. Lett.*, 2016,11(1): 420-1-7.

[32] KUANG W J, LIU X, LI Q, *et al*. Solution-processed solar-blind ultraviolet photodetectors based on ZnS quantum dots [J]. *IEEE Photon. Technol. Lett.*, 2018,30(15): 1384-1387.

[33] XIA Y, ZHAI G M, ZHENG Z, *et al*. Solution-processed solar-blind deep ultraviolet photodetectors based on strongly quantum confined ZnS quantum dots [J]. *J. Mater. Chem. C*, 2018,6(42): 11266-11271.

[34] CHENG S D, HAN S C, CAO Z Y, *et al*. Wearable and ultrasensitive strain sensor based on high-quality GaN pn junction microwire arrays [J]. *Small*, 2020,16(16): 1907461-1-8.

[35] GONG C H, CHU J W, QIAN S F, *et al*. Large-scale ultrathin 2D wide-bandgap BiOBr nanoflakes for gate-controlled deep-ultraviolet phototransistors [J]. *Adv. Mater.*, 2020,32(12): 1908242-1-9.

[36] KIM J H, RHO H, KIM J, *et al*. Raman spectroscopy of ZnS nanostructures [J]. *J. Raman Spectrosc.*, 2012,43(7): 906-910.

[37] HO C H, VARADHAN P, WANG H H, *et al*. Raman selection rule for surface optical phonons in ZnS nanobelts [J]. *Nanoscale*, 2016,8(11):5954-5958.

[38] XIONG Q H, CHEN G, ACORD J D, *et al*. Optical properties of rectangular cross-sectional ZnS nanowires [J]. *Nano Lett.*, 2004,4(9):1663-1668.

[39] VIRIEUX H, LE TROEDEC M, CROS-GAGNEUX A, *et al*. InP/ZnS nanocrystals: coupling NMR and XPS for fine surface and interface description [J]. *J. Am. Chem. Soc.*, 2012,134(48):19701-19708.

[40] RAMACHANDRAN K, JEGANATHAN C, KARUPPUCHAMY S. Surfactant assisted electrochemical growth of ultra-thin CuSCN nanowires for inverted perovskite solar cell applications [J]. *Org. Electron.*, 2021,95:106214-1-9.

[41] TSAI C T, GOTTAM S R, KAO P C, *et al*. Improvement of OLED performances by applying annealing and surface treatment on electro-deposited CuSCN hole injection layer [J]. *Synthetic. Met.*, 2020,269,116537-1-8.

[42] JIANG H, PENG H, GUO H, *et al*. Interfacial mechanical strength enhancement for high-performance ZnS thin-film anodes [J]. *ACS Appl. Mater. Interfaces*, 2020,12(46):51344-51356.

[43] DAI L W, STRELOW C, KIPP T, *et al*. Colloidal manganese-doped ZnS nanoplatelets and their optical properties [J]. *Chem. Mater.*, 2021,33(1):275-284.

[44] HASSAN S, BERA S, GUPTA D, *et al*. $MoSe_2$-Cu_2S vertical p-n nanoheterostructures for high-performance photodetectors [J]. *ACS Appl. Mater. Interfaces*, 2019,11(4):4074-4083.

[45] 张旭. 降低Si基有机光电探测器暗电流的研究 [J]. 甘肃科学学报, 2009,21(4):54-57.

ZHANG X. Study on the reduction of the dark current in Si-based organic photodetector [J]. *J. Gansu Sci.*, 2009, 21(4): 54-57. (in Chinese)

[46] CAI J, XU X J, SU L X, *et al*. Self-powered n-SnO_2/p-CuZnS core-shell microwire UV photodetector with optimized performance [J]. *Adv. Optical. Mater.*, 2018, 6(15): 1800213-1-7.

[47] WANG Y C, WU C, GUO D Y, *et al*. All-oxide NiO/Ga_2O_3 p-n junction for self-powered UV photodetector [J]. *ACS Appl. Electron. Mater.*, 2020, 2(7): 2032-2038.

[48] DAI W, PAN X, CHEN C, *et al*. Enhanced UV detection performance using a Cu-doped ZnO nanorod array film [J]. *RSC Adv.*, 2014, 4(60): 31969-31972.

[49] XIN B, WU Y T, LIU X R, *et al*. High performance UV photodetector based on 2D non-layered $CuGaS_2$ nanosheets [J]. *Semicond. Sci. Technol.*, 2019, 34(5): 055007-1-5.

[50] AGGARWAL N, KRISHNA S, SHARMA A, *et al*. A highly responsive self-driven UV photodetector using GaN nanoflowers [J]. *Adv. Electron. Mater.*, 2017, 3(5): 1700036-1-7.

魏瑶琪(1996-),女,江西上饶人,硕士研究生,2019年于东华理工大学获得学士学位,主要从事光电探测器方向的研究。

E-mail: wyq_kikiemail @163.com

韩三灿(1989-),女,山东济宁人,博士,讲师,2016年于复旦大学获得博士学位,主要从事光电半导体材料及器件的研究。

E-mail: mickey3can@163.com